PHYSICAL REVIEW B **88**, 081406(R) (2013)

Magnetic-field-controlled vacuum charge in graphene quantum dots with a mass gap

P. A. Maksym
Department of Physics and Astronomy, University of Leicester, Leicester LE1 7RH, United Kingdom

H. Aoki
Department of Physics,University of Tokyo, Hongo, Tokyo 113-0033, Japan

(Received 12 November 2012; revised manuscript received 7 March 2013; published 26 August 2013)

The effect of a magnetic field on the charged vacuum is investigated. The field dependence of the energy levels causes jumps in the total vacuum charge that occur whenever an energy level crosses the Fermi level, and this leads to reentrant cycles of vacuum *charging and discharging*. In atomic systems these effects require astrophysical magnetic fields of around 10^8 T, but in graphene with a mass gap they occur in laboratory fields of about 1 T or lower. It is suggested that an electrostatic graphene quantum dot defined by a gate electrode provides a solid state model of the as yet unobserved charged vacuum as well as a model of an atomic system in an extreme astrophysical environment. Phase diagrams are computed to show how the total vacuum charge depends on the confining potential strength and applied magnetic field. The vacuum charge density is also investigated and experimental consequences are discussed.

DOI: 10.1103/PhysRevB.88.081406 PACS number(s): 73.22.Pr, 31.30.J−, 73.21.La

The long-sought-for charged vacuum[1,2] is the ground state of strong field quantum electrodynamics (QED). Usually the vacuum is neutral but it charges in the presence of an electric field strong enough to lower a bound state into the negative energy continuum. For example, when the charge on the nucleus of a hydrogenic atom increases to beyond $\simeq$172, the 1s state enters the negative energy continuum and the vacuum charges. This is accompanied by spontaneous emission of two positrons which would enable the effect to be observed if a strong enough field could be created. In principle, this is possible because the critical charge can be exceeded in a collision between two uranium nuclei. But the interaction time is too short to allow the transition to a charged vacuum to occur[3] and, despite much effort, vacuum charging still needs to be observed. However, it may be possible to observe it in a semiconductor analog.

The band gap of a semiconductor is analogous to the mass gap of an atomic system and semiconductor quantum dots are analogous to natural atoms.[4] In electrostatic quantum dots, electrons are confined by an electrostatic potential that is generated by a gate electrode and replaces the Coulomb potential of a natural atom. Normally the dot is engineered so that the confined electron energies are just below the edge of the conduction band. But in a material with a small band gap it should be possible to use a stronger potential to lower a state into the valence band and create a charged vacuum analog.

Any material that allows a state to be lowered into the valence band with a modest gate voltage is suitable. One candidate is monolayer graphene on substrates that induce a gap, for example, BN,[5] Ru,[6] and, controversially, SiC.[7] Other candidates include semiconducting carbon nanotubes and narrow gap semiconductors. Graphene is the only candidate with a Dirac-like energy dispersion and hence the candidate that provides the most precise analog of QED. Indeed, it has already been suggested that a charged vacuum occurs in graphene in the presence of a Coulomb impurity with enough charge,[8] but it may be difficult to vary the impurity charge experimentally. However, *any potential attractive to electrons* and of sufficient strength charges the vacuum. This means a graphene quantum dot is an accurate and practical analog of the atomic charged vacuum. In addition, dots made of materials with nonrelativistic energy dispersion may allow studies of unusual charged vacua whose properties differ from the atomic one.

But the most interesting feature of the quantum dot analog is that the charged vacuum is extremely sensitive to an external magnetic field. A rough estimate of the field needed to cause significant effects may be obtained by equating the rest mass energy to the cyclotron energy. For atomic electrons this gives about 10^{10} T, an ultrastrong magnetic field that only occurs in extreme astrophysical environments such as magnetized neutron stars.[9] In contrast, for graphene with $m_0c^2 \sim 100$ meV and $c \sim 10^6$ ms^{-1}, the same estimate gives about 10 T, well inside the laboratory regime.

Moreover, important effects already occur at lower fields. Depending on their quantum numbers, energy levels both rise and fall as the magnetic field increases. If the energy of a charge carrying state rises above the Fermi level, the vacuum *discharges* while it *charges* if the energy of a state falls below the Fermi level. This leads to *reentrant* cycles of vacuum charging and discharging. The relevant energy scale for these processes is the depth of the state in the continuum. For a hydrogenic atom with $Z = 172$ this is about 15 keV (Ref. 2) and the field needed to discharge the vacuum is about 10^8 T, still in the astrophysical regime, while for a graphene quantum dot it is $\lesssim$1 T. These processes do not seem to have been investigated before and are studied here in the context of a graphene quantum dot. But the wave equation for a graphene dot is just the Dirac equation so *exactly* the same physics should occur in atomic systems in ultrastrong magnetic fields. The graphene dot is not only an analog of the charged vacuum but also an analog of atomic physics in extreme astrophysical environments.

The objectives of this Rapid Communication are, first, to demonstrate that charged vacuum states occur in graphene quantum dots, second, to demonstrate magnetic-field-induced

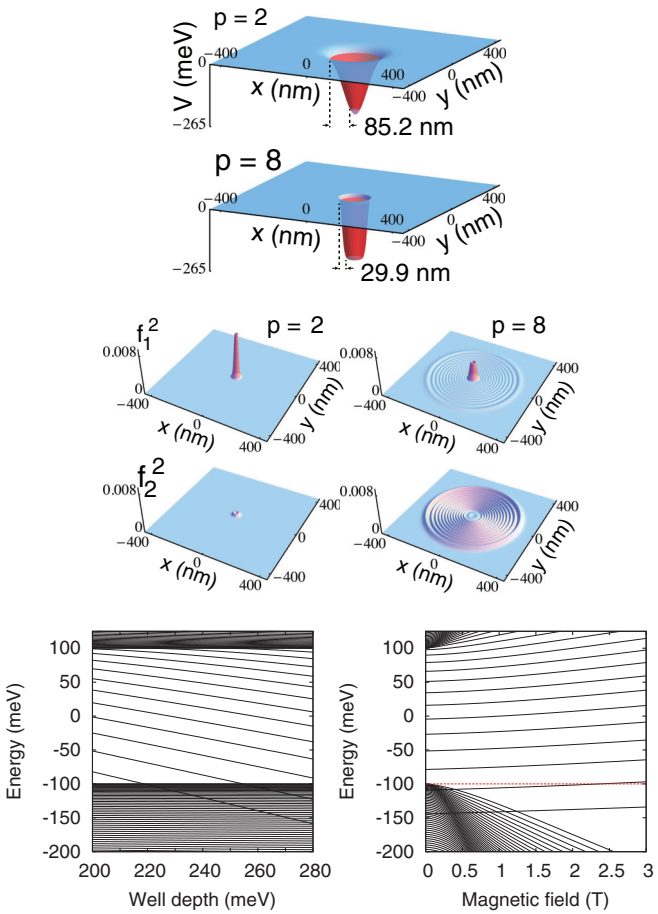

FIG. 1. (Color online) Model potentials (top); well depth and field dependent energy levels (bottom) and typical states at 0.704 T (center).

vacuum charging and discharging, and finally to consider the experimental consequences. The dot is taken to be circularly symmetric and the dot potential is modeled by $V(r) = V_0 \exp[-(r/\lambda)^p/2]$, where r is the radial coordinate, $|V_0|$ is the well depth, and $\lambda = 50$ nm is its width. p determines the shape and slope of the well; the bottom flattens and the edge sharpens as p increases (Fig. 1, top). The Gaussian form is convenient but not essential to the physics. The magnetic field B is taken to be uniform and perpendicular to the dot plane. The physics is within the range where the graphene dispersion relation is linear, so the Dirac particle picture is applicable and the quantum states are found from a two-dimensional effective mass equation. Interestingly, the reduced spatial dimensions may make it easier to realize a charged vacuum.[10] The mass is generated by including a site-dependent splitting parameter in the Hamiltonian, the same approach as in earlier work on graphene with a mass gap.[8,11]

The effective mass Hamiltonian for graphene consists of two 2×2 blocks which together are equivalent to the four-component Dirac Hamiltonian. One block gives the states near the K point of the Brillouin zone and the other gives the states near K'. The states near K are obtained from the two-component Hamiltonian $H = (\gamma/\hbar)\boldsymbol{\sigma} \cdot (\mathbf{p} + e\mathbf{A}) + V + m_0c^2\sigma_z$, where the $\boldsymbol{\sigma}$ are Pauli matrices, $\mathbf{p}$ is the momentum, and $\mathbf{A}$ is the magnetic vector potential. Here $c = \gamma/\hbar$, γ is taken to be 646 meV nm,[12] and m_0c^2 is taken to be 100 meV, the upper end of the observed range (10–100 meV). The eigenstates of a circularly symmetric dot are $\phi(\mathbf{r}) = \{\chi_1(r)\exp[i(m-1)\theta], \chi_2(r)\exp(im\theta)\}$, where θ is the azimuthal angle and m is the total angular momentum quantum number. Equations for the radial functions are obtained by making the substitutions $f_1 = \sqrt{r}\chi_1$, $if_2 = \sqrt{r}\chi_2$. This leads to

$$\frac{V + m_0c^2}{\gamma} f_1 + \left(\frac{d}{dr} + \frac{m - \frac{1}{2}}{r} + \frac{e}{\hbar}A_\theta\right) f_2 = \frac{E}{\gamma} f_1,$$

$$\left(-\frac{d}{dr} + \frac{m - \frac{1}{2}}{r} + \frac{e}{\hbar}A_\theta\right) f_1 + \frac{V - m_0c^2}{\gamma} f_2 = \frac{E}{\gamma} f_2.$$

These equations are discretized with a second-order forward-backward difference scheme[13] which leads to a real, symmetric eigenvalue problem that is solved numerically. The states near K' are found in a similar way. The numerical system radius is 600 nm.

Physically, the valley index is equivalent to a pseudospin and the states near K and K' correspond to pseudospin-up and pseudospin-down, respectively. The total angular momentum $\hbar(m - 1/2)$ is the sum of the orbital angular momentum and pseudospin. The orbital angular momentum quantum number $l = (m - 1/2) \pm 1/2$ is therefore $m - 1$ for states near K and m for states near K'.

Figure 1 shows the typical behavior of energy levels and quantum states. The bottom left frame shows the K energy levels as a function of well depth when $B = 0$, $m = 1$ (i.e., $l = 0$), and $p = 2$. Because of the finite system size the continuum consists of closely spaced discrete levels that form two bands with $|E| > m_0c^2$. The bound state levels occur in the gap between the two continua and plunge into the negative energy continuum as the well depth increases. Similar behavior is found for other values of m and p. The bottom right frame shows the K energy levels as a function of B for the same parameters as in the bottom left frame and well depth 265 meV. The continuum levels are now B dependent and the top of the negative energy continuum falls from ~ -100 meV at $B = 0$ T to ~ -200 meV at $B = 2.5$ T and within this field range the continuum levels remain closely spaced. In contrast, the bound state energies increase with B. Consequently, bound state levels that are in the negative energy continuum when $B = 0$ T move up as B increases. In particular, the bound state level closest to the continuum edge crosses $E = -m_0c^2$ (dashed line) when $B \sim 2.4$ T, and this corresponds to vacuum discharge in a system with a Fermi level $E_F \sim -m_0c^2$.

Typical states are shown in the center frame of Fig. 1. When a bound state enters the continuum, it hybridizes with the continuum states and forms a Fano resonance.[14] In the finite size numerical calculation this leads to a series of anticrossings where the bound state levels move through the continuum. Similar anticrossings have been found in earlier work on the vacuum charge.[2] Individual states that contribute to the resonance closest to the continuum edge are shown in the figure. The resonance width depends on the strength of the hybridization. Semiclassical analysis[15] shows that a forbidden region surrounds the dot. As shown by the arrows in Fig. 1, the

width of this forbidden region decreases when $p = 8$ and this strengthens the hybridization.[16] When $p = 2$, the resonance width is less than the numerical continuum level separation ($\sim$1 meV) and the resonance consists of one state. But when $p = 8$, it involves about two to four states. In the case of Fig. 1, B is chosen so that f_1 has roughly the same amplitude for the two main contributing states and the resonance width is about 3–4 meV. The corresponding state has a large peak in f_1 at the center, consistent with bound state character, and a ring of small oscillations that extends to about 300 nm, consistent with continuum character. This confirms that bound states can hybridize strongly with continuum states in a quantum dot. In contrast, strongly hybridized states do not normally occur in Coulomb potentials because the width of the forbidden region is large.

The vacuum charge density is the charge density induced in response to an external potential V. It may be found from QED charge density operators or directly and of course both ways give identical results.[17,18] The two equivalent QED operators are the normally ordered operator and the commutator operator $\hat{\rho} = (-e/2)[\bar{\psi}, \gamma^0 \psi]$, where γ^0 is a Dirac matrix, ψ is the Dirac field operator, and $\bar{\psi}$ is its adjoint. The more widely used direct expression is $\rho(V) - \rho(0)$, where the charge density ρ is found by summing over states below E_F. In the present work $\hat{\rho}$ is used to ensure that the calculation parallels earlier work on the vacuum charge[2] and because this is more efficient than the direct approach. Integrating the the vacuum expectation value of $\hat{\rho}$ gives the total vacuum charge $Q = (-e/2)(\sum_{E_n < E_F, \alpha} - \sum_{E_n > E_F, \alpha})$. In QED the sums in $\hat{\rho}$ and Q are divergent and have to be treated with charge renormalization, but they are convergent in the present numerical model because the energy spectrum is bounded.

The total vacuum charge as a function of well depth and magnetic field is shown in Fig. 2. Real-spin splitting is included and the effective g factor is taken to be 2.0. E_F is taken to be just above $-m_0c^2$ so all real-spin-split Landau levels remain below it, and this choice corresponds to the one used in atomic physics. For $B = 0$ the vacuum charge increases monotonically with well depth in a series of steps. The first step occurs when the $l = 0$ level shown in Fig. 1 enters the vacuum. Each step has height 4 and this corresponds to a twofold pseudospin degeneracy and a twofold real-spin degeneracy. At a constant well depth the vacuum charge as a function of B shows reentrant behavior for both values of p. For instance, for well depth 220 meV and $p = 2$, it falls when $B \sim 0.41$ T and

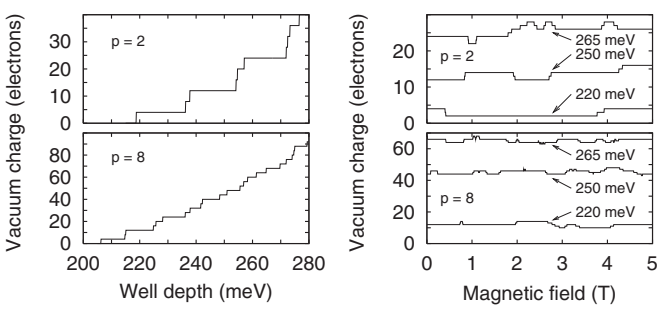

FIG. 2. Total vacuum charge as a function of well depth (left) and magnetic field (right).

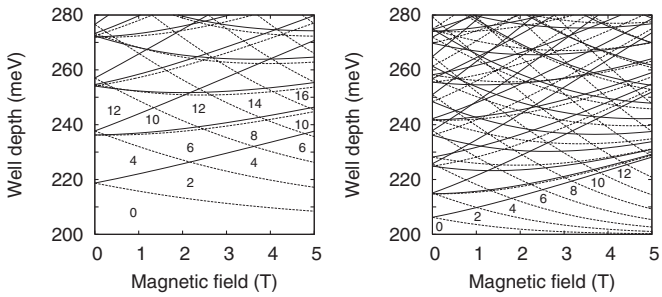

FIG. 3. Vacuum charge phase diagrams for $p = 2$ (left) and $p = 8$ (right). K phase boundaries solid, K' dashed.

then rises when $B \sim 3.9$ T. The fall occurs because the $l = 0$, K level leaves the continuum while the rise occurs because the $l = -1$, K' level enters the continuum. The behavior at a larger well depth is similar but richer because some levels go through a minimum as a function of B.[18] Another effect of the field is real-spin splitting. This allows an odd numbered vacuum charge and leads to double steps of height 1, for example, at $B \sim 3.9$ T with a well depth 220 meV and $p = 2$.

To investigate the details, vacuum charge phase diagrams are computed (Fig. 3). Each phase boundary indicates where an energy level E_n crosses the Fermi level and is given implicitly by $E_n(V_0, B) = E_F$. The total vacuum charge is shown on selected portions of the diagrams. For clarity, real-spin splitting is not included. Hence each line corresponds to a vacuum charge step of two electrons when $B \neq 0$ and four when $B = 0$. The results in Fig. 2 are sections through the phase diagrams with real-spin splitting included. The phase boundaries reflect the physics of the system: They have small splittings at $B = 0$, unless $l = 0$, and there is pronounced B-dependent splitting. These effects can be understood from the nonrelativistic limit of the effective mass equation. To order $1/m_0^2$ the splitting at $B = 0$ results from the pseudospin-orbit interaction and the B-dependent splitting results from the interaction of the pseudospin with the magnetic field. Quantitatively, the exact splittings at $B = 0$, $V_0 = -180$ meV, and $p = 2$ are 1.05, 1.88, and 2.49 meV for the lowest states at $l = 1$, 2, 3, respectively, while the lowest-order pseudospin-orbit splittings are 1.36, 2.57, and 3.63 meV. The B-dependent splitting at 1 T, calculated from the pseudospin g factor, is 6.33 meV while the exact splitting at $l = 0$ is 6.05 meV. Hence the nonrelativistic limit describes the physics qualitatively but the exact equation is needed to find the splittings accurately.

The vacuum charge density (Fig. 4) is very similar to the vacuum charge density found in atomic physics, and this confirms that the graphene vacuum charge is a precise analog of the one found in atomic physics.[2] The charge density increase associated with the charging steps is found from $\rho(V_0 + \delta V_0) - \rho(V_0)$, where δV_0 is small (-0.1 meV)—the numerical equivalent of the procedures used in atomic physics.[2] In atomic physics terminology, states below the threshold for vacuum charging are described as undercritical while those above it are called overcritical. Figure 4 shows the charge density associated with the first step at $B = 0$ T in Fig. 2. To a good approximation, the vacuum charge is stored in one overcritical state when $p = 2$ and two when $p = 8$. The open circles indicate the charge density computed from these

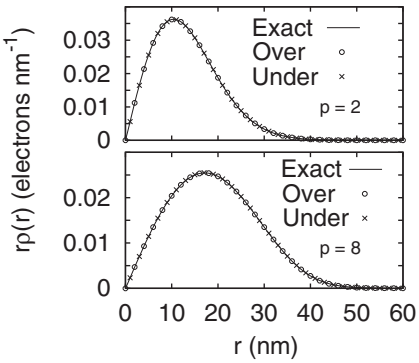

FIG. 4. Comparison of vacuum charge density and overcritical and undercritical state densities at $B = 0$ T.

few states. Near the peak they agree with the exact data to better than a few parts in 1000. This shows that the vacuum charge density is stored in a resonance as in the atomic case. In addition, the exact density is also approximated to similar accuracy by the undercritical bound state density (crosses), and this is the consequence of a sum rule similar to the one that applies in the atomic case.[2] This again suggests that graphene vacuum charge is an exact analog of the atomic one. However, the possibility of strongly hybridized states is a different feature that only occurs in graphene. In this case the resonance broadens and the figure shows the total density that would be observed with low energy resolution.

There are several experimental consequences of these findings. First, the vacuum charge in a graphene quantum dot may be detectable via emission of holes that is analogous to spontaneous positron emission. It may be possible to pump the gate voltage to enhance this effect. Second, the strong hybridization may be detectable with scanning tunneling spectroscopy (STS). Although the hybridization does not affect the density observed with low energy resolution, the states in Fig. 1 extend to a radius about an order of magnitude larger than the dot radius. They should be detectable when energies less than the width of the Fano resonance can be resolved and this requires temperatures of a few K. Third, it may be possible to detect the vacuum charge directly, for example, by capacitance measurements or quantum point contact electrometers. These experiments only require a gate that can take a bound state through a gap; perfect circular symmetry is not needed and the gap may be position dependent.[19] The ideal material for the experiments should be undoped or p doped to ensure that an empty state is taken through the gap and it should be graphene with a gap (the situation is different in gapless graphene[20]) to ensure that the effective mass equation is a precise analog of the Dirac equation. Existing results[5,6] suggest that a suitable material can be found. In addition, it should be possible to observe a charged vacuum analog in narrow gap semiconductors or semiconducting carbon nanotubes, although the effective mass equation is no longer relativistic.

In summary, a quantum dot in graphene with a mass gap provides an accurate model of the charged vacuum. The vacuum charge is strongly affected by a magnetic field and a sufficiently strong magnetic field can discharge the vacuum. These effects should also occur for atomic electrons in a magnetic field, but the small rest mass energy of graphene charge carriers allows them to be seen with fields $\sim$1 T instead of the extreme astrophysical fields needed for atomic electrons. Experimentally, it may be possible to detect the graphene charged vacuum directly, or by observation of hole emission or by probing the states with STS. The effect of interactions remains to be investigated, but a Thomas-Fermi approach[2] suggests the atomic vacuum charge survives the effect of interactions.

Recently, Wang *et al.*[21] and Luican-Mayer *et al.*[22] reported relevant experimental work. The experiments of Wang *et al.* involve the assembly of Ca dimer clusters in graphene on BN and manipulation of the number of dimers with scanning tunneling microscopy (STM). The experiments of Luican-Mayer *et al.* involve the use of magnetic-field-dependent screening to control the strength of the potential around a charged impurity.

We thank Seigo Tarucha, Michihisa Yamamoto, and Robin Nicholas for useful discussions. This work was supported by the UK Royal Society and the Japanese Ministry of Education, Scientific Research No. 23340112.

[1] S. Gershtein and Y. B. Zeldovich, Lett. Nuovo Cimento **1**, 835 (1969); W. Pieper and W. Greiner, Z. Phys. **218**, 327 (1969).

[2] W. Greiner, B. Müller, and J. Rafelski, *Quantum Electrodynamics of Strong Fields* (Springer, New York, 1985).

[3] R. Ruffini, G. Vereshchagin and S.-S. Xue, Phys. Rep. **487**, 1 (2010).

[4] P. A. Maksym, H. Imamura, G. P. Mallon, and H. Aoki, J. Phys.: Condens. Matter **12**, R299 (2000); L. P. Kouwenhoven, D. G. Austing, and S. Tarucha, Rep. Prog. Phys. **64**, 701 (2001); G. Giavaras, P. A. Maksym, and M. Roy, J. Phys.: Condens. Matter **21**, 102201 (2009); P. Recher, J. Nilsson, G. Burkard, and B. Trauzettel, Phys. Rev. B **79**, 085407 (2009); P. A. Maksym, M. Roy, M. F. Craciun, M. Yamamoto, S. Tarucha, and H. Aoki, J. Phys.: Conf. Ser. **245**, 012030 (2010); S. Schnez, K. Ensslin, M. Sigrist, and T. Ihn, Phys. Rev. B **78**, 195427 (2008).

[5] G. Giovannetti, P. A. Khomyakov, G. Brocks, P. J. Kelly, and J. van den Brink, Phys. Rev. B **76**, 073103 (2007); L. Ci, L. Song, C. Jin, D. Jariwala, D. Wu, Y. Li, A. Srivastava, Z. F. Wang, K. Storr, L. Balicas, F. Liu, and P. M. Ajayan, Nat. Mater. **9**, 430 (2010); C. Yelgel and G. P. Srivastava, Appl. Surf. Sci. **258**, 8342 (2012).

[6] C. Enderlein, Y. S. Kim, A. Bostwick, E. Rotenberg, and K. Horn, New J. Phys. **12**, 033014 (2010).

[7] S. Y. Zhou, G.-H. Gweon, A. V. Fedorov, P. N. First, W. A. de Heer, D.-H. Lee, F. Guinea, A. H. Castro Neto, and A. Lanzara, Nat. Mater. **6**, 770 (2007); L. Vitali, C. Riedl, R. Ohmann, I. Brihuega, U. Starke, and K. Kern, Surf. Sci. **602**, L127 (2008); A. Bostwick, T. Ohta, J. L. McChesney, K. V. Emtsev, T. Seyller, K. Horn, and E. Rotenberg, New J. Phys. **9**, 385 (2007); W. A. de Heer, C. Berger, X. Wu, M. Sprinkle, Y. Hu, M. Ruan, J. A. Stroscio, P. N. First, R. Haddon, B. Piot, C. Faugeras, M. Potemski, and J.-S. Moon, J. Phys. D: Appl. Phys. **43**, 374007 (2010).

[8] V. M. Pereira, V. N. Kotov, and A. H. Castro Neto, Phys. Rev. B **78**, 085101 (2008).

[9]D. Lai, Rev. Mod. Phys. **73**, 629 (2001).
[10]H. Katsura and H. Aoki, J. Math. Phys. **47**, 032301 (2006).
[11]G. Giavaras and F. Nori, Phys. Rev. B **83**, 165427 (2011).
[12]R. Saito, G. Dresselhaus, and M. S. Dresselhaus, *Physical Properties of Carbon Nanotubes* (Imperial College Press, London, 1998).
[13]G. Giavaras, P. A. Maksym, and M. Roy (unpublished).
[14]U. Fano, Phys. Rev. **124**, 1866 (1961).
[15]P. A. Maksym and G. Giavaras (unpublished).
[16]See Supplemental Material at http://link.aps.org/supplemental/10.1103/PhysRevB.88.081406 for examples of forbidden region width; see also P. Carmier and D. Ullmo, Phys. Rev. B **77**, 245413 (2008); A. Kormanyos, P. Rakyta, L. Oroszlany, and J. Cserti, *ibid*. **78**, 045430 (2008).
[17]J. D. Bjorken and S. D. Drell, *Relativistic Quantum Fields* (McGraw-Hill, New York, 1965).
[18]P. A. Maksym and H. Aoki, J. Phys. Conf. Ser. **456**, 012026 (2013).
[19]B. Sachs, T. O. Wehling, M. I. Katsnelson, and A. I. Lichtenstein, Phys. Rev. B **84**, 195414 (2011).
[20]V. M. Pereira, J. Nilsson, and A. H. Castro Neto, Phys. Rev. Lett. **99**, 166802 (2007); A. V. Shytov, M. I. Katsnelson, and L. S. Levitov, *ibid*. **99**, 246802 (2007).
[21]Y. Wang, D. Wong, A. V. Shytov, V. W. Brar, S. Choi, Q. Wu, H. Tsai, W. Regan, A. Zettl, R. K. Kawakami, S. G. Louie, L. S. Levitov, and M. F. Crommie, Science **340**, 734 (2013).
[22]A. Luican-Mayer, M. Kharitonov, G. Li, C. Lu, I. Skachko, A. B. Goncalves, K. Watanabe, T. Taniguchi, and E. Andrei (unpublished).